Infinite Science | Publishing

Topology Optimization and Manufacturing of Engine Bracket using Electron Beam Melting

Murat Isik[1,2]*, Erdal Kisa[1,2], Bahattin Koc[1,2,3], Mehmet Yildiz[1,2,3], Baris Pehlivanogullari[4], Akin Orhangul[4], Guray Akbulut[4]

[1]*Integrated Manufacturing Technologies Research and Application Center, Sabanci University, Orhanli-Tuzla, 34956 Istanbul, Turkey*
[2]*Composite Technologies Center of Excellence, Sabanci University-Kordsa, Istanbul Technology Development Zone, Sanayi Mah. Teknopark Blvd. No: 1/1B, Pendik, 34906 Istanbul, Turkey*
[3]*Faculty of Engineering and Natural Sciences, Sabanci University, Orhanli-Tuzla, 34956 Istanbul, Turkey*
[4]*TUSAS Engine Industries Inc., 26003, Eskisehir, Turkey*
Corresponding author, email: murat.isik@sabanciuniv.edu

Abstract

Nickel-based alloys are widely used for aerospace applications since they exhibit tremendous mechanical strength under extreme conditions. Additive manufacturing (AM), especially electron beam melting (EBM), is of interest due to its potential of direct digital manufacturing of highly complex fully functional light-weight critical components such as engine brackets. Primary tasks of the brackets, are to damper the vibration and support the engine weight. Therefore, it is critical to simultaneously reduce its weight and maintain good mechanical properties. Topology optimization is commonly used for this purpose. In this study, the reference and topologically optimized brackets are fabricated via EBM method, and then followed by subjecting to the hot isostatic pressing (HIP) procedure. The weight of the engine bracket is reduced by 32% utilizing finite element analyses (FEA) based topology optimization. Furthermore, the effect of different loading conditions is tested on the topologically optimized and EBM-built Inconel 718 bracket. The reference and topologically optimized brackets are subjected to the tensile tests using a custom-made fixture and the area under the 'Load vs. Tensile Extension' curves are estimated to obtain average energy values using software where a 16.3% energy increase is witnessed.

Keywords: Nickel-based alloys, Additive manufacturing, bracket, Topology optimization, Finite element analysis, Tensile tests.

1. Introduction

Recently, nickel-based superalloys, predominantly Inconel 718 have created significant impact on the aerospace parts such as shafts, turbine discs, and blades due to their excellent strength and fatigue life, good corrosion, oxidation, and radiation resistance [1–3]. There are numerous studies in the literature regarding Inconel 718 alloys commonly processed with conventional production methods such as casting, forging [4] and machining [5]. Nevertheless, conventional production methods are limited to manufacturing simple geometries and there are still unmet needs in manufacturing complex parts. Additive manufacturing (AM) technologies such as, directed energy deposition [6–8], selective laser melting and electron beam melting, have attracted massive attention recently as it retains numerous advantages over conventional manufacturing technologies [1,9]. AM has already been adopted by aerospace companies, by offering reliable manufacturing of complex parts, with no or a little need of machining processes [10,11]. Further, AM improves the production rate in a cost-efficient manner while at the same time enabling innovative and light-weight designs [12–14] using topology optimization (TO) [15,16]. TO broadly attracts the attention of industry and academic society to determine the best structural configuration of the functional parts [17,18] and to calculate the optimal material distribution inside a design domain for light-weighting [19]. Conventional production methods usually struggle or fail to achieve the designs requiring from TO methods due to challenges of fabricating complex geometries and shapes [20]. It is envisioned that utilizing a combination of TO and AM is an efficient way to fabricate high performance critical parts while reducing the weight [21,22]. Among the TO methods, structural TO has been the one of the most efficient way to use in the field of aerospace while in a limited number of study thermo-elastic TO has been practiced [23,24]. Application examples of the TO application in the literature are abundant. There have been several researches are focused on TO introduction to the lattice structures aiming to obtain the knowledge related to application of ultra-light components [25,26]. Aside from this, some of the TO researches are focused on AM constrains. Researchers investigated the overhang

constrain in TO for self-supporting as well. Unfortunately, the studies concerned to TO application to the real functional parts and comprehensive verification of TO using experimental methods are still limited. For example, Shi et al. have conducted a thermo-elastic TO study on titanium bracket using another type of powder bed fusion manufacturing method (selective laser melting) [23]. Adopting the TO, efficient weight reduction on a part is applicable and have examples in industry. For instance, a previous work on an engine component of Airbus A320 has been reported to have as high as a 64% mass reduction, when compared to the original design [23]. Similarly, Airbus has achieved 35% lighter aluminum structural bracket for satellite applications (Eurostar E3000) [25]. European Space Agency (ESA) has applied the TO on Sentinel 1 Upper S-Band Antenna bracket where an almost 42% weight reduced design has been succeeded [25]. However, the mechanical performance of the weight-reduced bracket has not been mentioned in none of above-mentioned studies. Moreover, the studies solely conducted TO without mechanical tests, the interest of target mechanical property and its origin also vary. For instance, Talay et al. has achieved TO on AlSi10Mg alloy automotive engine bracket 37% weight reduction, produced by high-pressure die casting method, and investigated the effect of stress originated from vibration [15]. Optistruct software has been used for the TO whereas the volume of design space has been mainly created with 3D hexagonal elements in the referred study. The bracket weight has been aimed to be decreased without violating constraints coming from modal and static analyses. Even in this example, the demand of examining the effect of a statical force on the bracket's performance subsequent to TO has not been met. Not only this but there is also a shortage of a thorough and comprehensive study in the literature consisting of TO application to a bracket, the assessment of its mechanical performance via a combination of simulations and experimental methods. The previous literature examples regarding critical functional parts have been concerned on simply modelling and simulation. Beyond this, and in general, there is a scant of literature concerning TO of additively manufactured aerospace engine components, and their characterization.

In this study, structural TO of and Inconel 718 bracket manufactured using electron beam melting (EBM) AM is the main focus. An aerospace bracket is designed through structural TO and fabricated using EBM. It is hypothesized that the tensile tests on topologically optimized bracket will promote us to understand the real-life validity and practicability of the designed concept. Understanding the TO and mechanical properties of the EBM-made Inconel 718 bracket will contribute to the potential substitution of conventional fabrication methods with AM in the future, and boost its real-world applications.

2. Material and methods

2.1. Finite element analysis of bracket

The initial weight of the reference engine mounting bracket is calculated to be 1.1509 kg before applying topology optimization (TO). Sequential Convex programming method was employed for topology optimization analyses. Hex20 elements are selected in the finite element analysis (FEA) of brackets using ANSYS software [27]. Each element is defined by 20 nodes having three degrees of freedom (ux, uy and uz) per node. The output of the analyses was confirmed by means of using mesh count. The optimum mesh count was estimated using mesh convergence with a 1% convergency rate. Overhang angle constraint is chosen as 45° from building plate. The minimum feature size or unit length is set 1 mm. A load of 20 kN is applied with angles such as 0°, 45°, 60°, 75° and 90°. The bracket holes are constrained in 6 degrees of freedom in 3D space as the boundary condition. The manufacturing constraint is set symmetrical. 3 mm minimal unit length is determined another boundary condition. Regarding the mesh structure of hole structures, inflation is used. Material properties of the Inconel 718 bracket are designated orthotropic-elastic since materials manufactured using additive manufacturing exhibit anisotropic microstructure and mechanical properties. Density, elastic modulus, Poisson's ratio and shear modulus values are used 8220 kg/m3; Ex:149 GPa, Ey:149 GPa and Ez:125 GPa; vx:vy:vz: 0.3; and Gx: 57.3 GPa, Gy: 57.3 GPa and Gz:48.07 GPa.

2.2. Production of Inconel 718 engine brackets with EBM

Inconel 718 alloy brackets are manufactured using an electron beam melting (EBM) (Arcam A2X system, Sweden) set up. The Inconel 718 powder (with a size distribution ranges from 45 to 106 μm) is used for this study. The samples are produced using a steel base plate where it is preheated up to 1023 °C, and this temperature is kept constant throughout the process. Arcam EBM software is used to generate zigzag pattern scanning strategy for the standard melt theme of Inconel 718 for processing of the brackets. The initial weight of the manufactured reference and topologically optimized brackets are measured 1.155 kg and 0.784 kg, respectively, implying a 32% mass reduction; 30% weight reduction has been aimed at the volumes where the stress distribution is low according to FEA analyses and the target stress values have been determined to be ±12% of the stress value of the reference bracket (337,7 MPa). After additive manufacturing of the brackets, they are subjected to hot isostatic pressing (HIP) procedure subsequent to EBM fabrication. The solution heat treatment is performed at 954 °C for 1 h, followed by rapid cooling to the room temperature. Subsequently, the double aging heat treatment consisting of holding at 718 °C for 8 h, followed by furnace cooling to 621 °C and maintaining at 621 °C for 10 h, and finally rapid cooling to room temperature, is realized. Hereafter reference

bracket and topologically optimized brackets are referred to as BR_{ref} and BR_{To}.

2.3. Mechanical tests

Tensile properties of the brackets are evaluated at room temperature using an Instron type (Instron 8853, 250 kN/2000Nm) testing machine in the current study. For locating maximum strained regions on the bracket and therefore using this information for the mounting the strain gauges, a tensile test using digital image correlation (DIC) is conducted at 35 kN. The tensile tests are applied with a cross-head speed of 0.5 mm/min. At least five tensile test measurements are taken from each bracket to calculate an average value of energy. A commercial type Instron Bluehil® software is used to estimate the area under the 'Load vs.Tensile Extension' curves.

3. Results and discussion

The finite element method (FEM) is [28] utilized to solve partial differential equations in two or three space variables (e.g. boundary value problems). To simply solve the problem of what is the best configuration to accommodate the load while reducing weight of the engine bracket, the FEM-based topology optimization is used. For the FEM analysis, the number of the elements is an important factor that contributes the accuracy, computational time, design domain size and material distribution [29,30]. Moreover, the correlation between the design domain size and material distribution crucially matters as well. Considering these aspects, each element is designed as 1 mm in the current study. Fig. 1 presents mesh structure of the bracket. Mesh structure is known to be a discrete symbol of the geometric model, and is expected to carry significant impact in the final solution. Differentiation of topology structures depending element size and mesh size studies are reported by the previous scholars [29,31] where the finer meshes has been required smaller element sizes. Although a very fine element size about 1 mm is employed during the element adding procedure, a 3 mm element size is used for removal to ensure faster computational time. 45° overhang angle is used as the manufacturing constrain. The total count of the elements and nodes used in the FEA are 138984 and 608464, respectively. The element type used in the simulations is known for also having significant impact on the results. It is reported and observed prior; the most widely used elements in FEA are the tetrahedrons and hexahedrons [32]. Hex20 element has been preferred due to its convenience to determine the stress concentrations on the surface of the engine bracket during the elastic calculations. Besides, Hex 20 element is capable of modelling the curved edges and uneven shapes whereas not detreating the sensitivity. Another reason for the hexagonal element's selection in the current study is due to fact that they also give rise to more accurate results, though they are avoided to be used in the complex structures [15]. This is because solving linear system equations using Hex20 takes longer time due to higher number of degrees of freedom and slower overall convergence rate compared to the other elements [33]. When the element count and type used are compared across to the previously reported literature, for instance Talay et al., use of almost tetragonal 225 000 elements, which has been known to have the possibility of giving less accurate analysis results when compared to the use of Hex20 element, and is also almost twice of what is used for the current study [15]. Apart from the element count and type used in the analyses, the differences in the node number of a specific element type, relationship between the selected element type, the model geometry, and mesh generation are reported to have vital importance on the static analysis result [32,34].
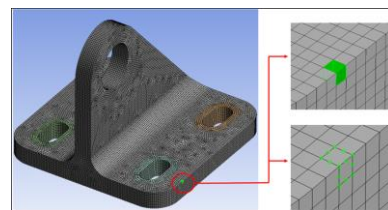

Fig 1. Mesh structure of the bracket.

The bracket is subjected to a constant 20 kN load with five different angles (0°, 45°, 60°, 75° and 90°) through the FEA as seen in Fig. 2 (a). The red-colored surfaces have constraints to the six degrees of movement in the space under loading conditions as shown in Fig. 2 (b). These red-colored regions are exclusively paid attention and avoided from light-weighting procedure since they will be used for fixing the brackets to the designed fixture during the tensile tests [23]. The symmetry is assigned to the bracket in the directions of z and y axes as displayed in Figure 2 (c). To define the material properties of Inconel 718 subjected to EBM followed by HIP, tensile tests are conducted and data obtained from the mechanical tests are used for the FEA.
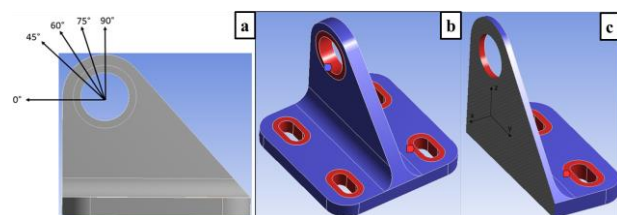

Fig 2. a) Loading directions, b) Restricted regions and c) Boundary conditions for structure symmetry during the FEA analyses of the bracket.

The TO is known to be an iterative process. Subsequent to definition of the base optimization set-up, the variables are adjusted until the solution reaches the pre-determined targets in the preliminary analysis, for example, necessary stress levels or weight reduction. Following the optimization, the strategy of the solution interpretation and modelling are defined. A comparison between the optimized component design and TO solution is done to confirm this strategy. The final

design of the optimized component is analyzed using FEA to validate stress levels, to check the highly stress concentrated regions and to find where the material reinforcement is necessary.

Figure 3a shows the designed testing fixture and its finite element structure. A total count of the nodes and elements used in the mesh creation are 4.250.774 and 1.001.112, respectively. The fixture is designed considering the aspects such as a successful mounting of the bracket to tensile testing machine, and the testing load. Besides, considering the hardness of the Inconel 718 brackets, the fixture is necessary to be made of a material harder than the Inconel 718, such as tool steel (DIN 1.2344), to suppress the possibility of any crushing phenomenon. The designed fixture for the tensile tests of the brackets is, as shown in Fig. 3b, used for both FEA and real-life experiments. M10 and M26 bolts are pre-loaded with 20 kN and 80 kN, respectively. The load value, 35 kN, along the z direction is pre-determined considering the stress-strain curve of Inconel 718 material. The reason for preferring this load is due to fact that the Inconel 718 made-bracket will operate in a load range within the elastic region of the material.
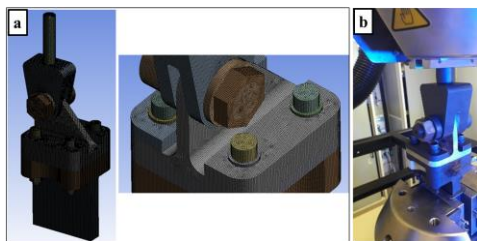

Fig 3. a) Finite element structure of the fixture model for tensile tests simulations b) manufactured fixture based on FEA design and mounted on tensile testing machine.
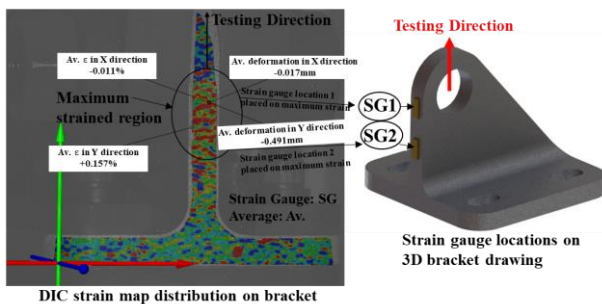

Fig 4. DIC strain map on the bracket and determination of strain gauge locations on the bracket.

Based on DIC test results, the maximum strain is obtained at the region inside the black circle of Fig. 4. where the average deformation and strain are 0.491 mm and 0.157%, respectively. These regions are decided to be used as locations to place strain gauges for the FEA modeling and tensile tests using strain gauge. Two of the strain gauges are placed as shown in Fig. 4 and they are referred to as SG1 and SG2 for strain gauges 1 and strain gauges 2, respectively. Using the valuable information of regarding where the maximum strain locates on the bracket, FEA are conducted on

BR_{ref} and BR_{To} (see the final geometry of BR_{To} in Fig 5.b). The strain distribution on the strain gauges (SG2) during the tensile tests is shown in Fig. 6. The min. and max. strain values of BR_{ref} for S1 are found to be 0.0592% and 0.025% while they are 0,07027% and 0,05357% for S2, respectively. In the case of BR_{To}, min. and max. strain values are 0,06271% and 0,02509% for S1 whereas they are 0,07156% and 0,05376% for S2, respectively. The increase in the maximum strains is found to be 5.91% and 1.85%, respectively, for the S1 and S2.
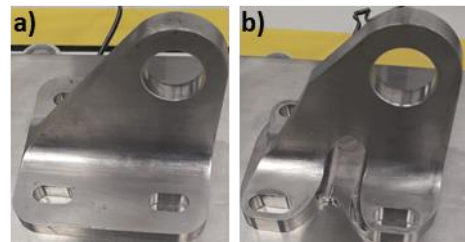

Fig 5. Captured images of a) reference b) topologically optimized bracket.

To confirm the FEA analysis, tensile tests are realized using strain gauges at 25 kN load. The average strain values of S1 are found to be 0.0567% and 0.0598%, respectively, recommending a 5.47% strain increase with the TO introduction. This value suggests only an 8% deviation between theoretical and experimental values for S1. For the case of S2, the average strain values are 0.08716 and 0.0849, respectively demonstrating a 2.59% strain increase in the bracket upon the TO introduction. When the strain increase for the experimental value compared to the what was obtained by the FEA, it is perceived that there is a 40% deviation between theoretical and experimental data. This could be due to fact that when the maximum strain is greater in a location, it causes an extended difference between FEA result and the measured strain gauge data; S2 yields higher values of strain based on FEA and the test conducted using strain gauges.

Figure 7 represents the FEA of the tensile test. The maximum total deformation along the Y axis for the BR_{ref} and BR_{To} are 0.142 mm and 0.143 mm, respectively, meaning there is no significant change in the maximum deformation on the brackets upon the TO. However, a larger portion of area on the vicinity of the internal hole is subjected to deformation pertained at BR_{To}. The deformation values steadily decrease from top of the internal holes to the ground in diagonal direction. Unlike this phenomenon, the total equivalent strain and stress exhibit a more unique pattern when compared to deformation at Y axis values. When the current study is compared across the previously reported literature, Shi et al. reported the maximum deformation of the SLM-fabricated titanium reference and topologically optimized brackets are around 0.907 mm and 0.659 mm, respectively [23]. The location of the maximum deformation is similarly located around the internal hole, which is at the top region of the bracket. The gradual decrease of the deformation levels

Infinite Science | Publishing

from internal holes to the direction of the ground levels of the bracket is observed, as it is also shown in the current study. When compared across to previously published literature by Shi et al. [23], an almost 27.3% deformation decrease is calculated upon the application of TO. As opposite of this behavior, almost no change in the maximum deformation is observed in the current study.
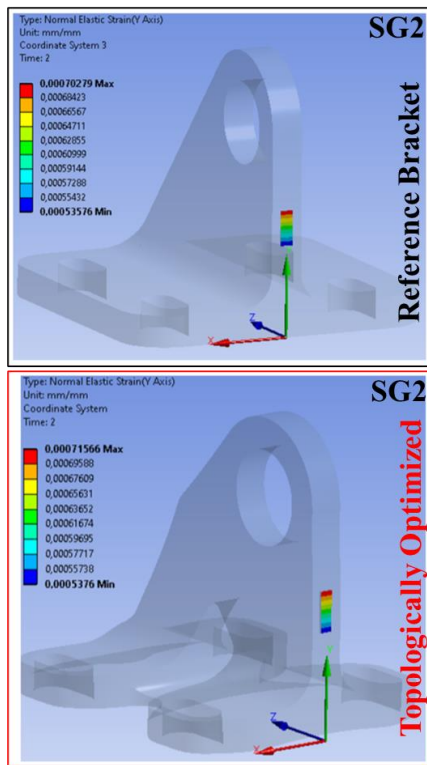

Fig 6. FEA analyses on the bracket showing elastic strains of the regions where the maximum strain is obtained based on DIC test.

The total strain values of reference and topologically optimized bracket are 0.00277 mm/mm and 0.00340 mm/mm, respectively. The regions showing maximum strain around the internal hole is located perpendicular to the loading direction and continuously decreases along the axis. The frontier and bottom of the reference bracket are in a strain-free state, when the topologically optimized bracket is entirely strained. This is 22.7% strain increase following the TO based on modeling of the tensile test on bracket and which is much greater than what is obtained by the FEA results conducted on S1 and S2 strain gauges demonstrating a 5.91% and 1.85% strain increase, respectively.

The maximum equivalent stress of the BR_{ref} and BR_{To} are 337.7 MPa and 372.4 MPa, respectively; that is a 10.3% increase in the stress when the BR_{ref} is weight reduced via FEA. The stress distribution images of the BR_{ref} and BR_{To} conditions are almost analogues of the total strain distribution images. In comparison to the previously reported literature, it is found that the maximum von-Mises stress of the reference and optimized brackets are 554.8 MPa and 636.4 MPa, respectively, and these values suggest an 14.7%

increase in the observed maximum stress value by Shi et al. [23]. The maximum stress observed in the current study (about 10.3%) is less than the what was reported by Shi et al. (about 14.7%). Moreover, the weight reduction is found 32% in the current study, and this is almost two times of the what was achieved by the Shi et al. This outcome can be attributed to several factors such as the type of the AM method, material intrinsic properties and the design strategy.
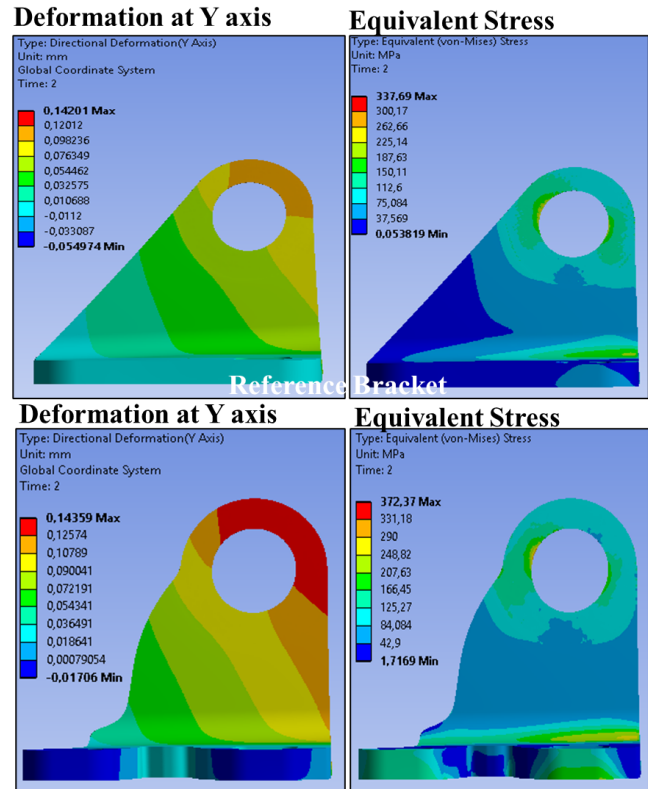

Fig 7. FEA analyses demonstrating bracket's deformation, and equivalent stress distribution.

Tensile tests using a tailor-made fixture are also carried out where only the jaw displacement is taken into account and no strain gauge is used. The mean absorbed energy values of the BR_{ref} and BR_{To} at 25 kN maximum load are 3153.5±69.1 J and 3663.6±69.1 J, respectively, recommending 16.3% energy increase upon the TO introduction to the BR_{ref}. The increase in the energy is a temporary phenomenon since the experiments are conducted in the elastic region; therefore, the absorbed energy during the loading equals to how much energy is released during the unloading [35,36]. It is an accepted knowledge that no energy is expected to be dissipated as heat in the elastic region [35,36] and the experiments of the current study are not realized in the plastic deformation region. When the total deformation values are checked for BR_{ref} and BR_{To}, which are 0.142 mm and 0.174 mm, respectively, it is realized that there is a total deformation around 21.8%. This shows that there is a proportional relation between the 22.7% and 21.8% strain (obtained by FEA) and total deformation increases, respectively. Judging by experimental test results and analysis data (taking the experimental total

strain increase as reference), it is possible to comment that FEA data can be verified via the experimental tests with an accuracy rate of 4.13% while it is 40% using the strain gauges at maximum strained region.

4. Conclusions

Inconel 718 made parts have crucial importance in the aerospace industry due to their exceptional performance under extreme conditions. There is only limited amount of study in the literature regarding the topology optimization (TO) of Inconel 718 brackets. In our current study, we introduced TO to the additively manufactured EBM Inconel 718 bracket, and simulated its deformation via FEA and compared with the reference bracket. Although, there has been some studies regarding on TO of the additively manufactured brackets using other methods, none of them focused on EBM Inconel 718 bracket, or simultaneously confirmed the analyzed functional part via experimental tests. The current study offers a comprehensive work combining FEA, and tensile tests on the brackets using a designed fixture. A 32% weight reduction is accomplished while only a 16.3% energy increase occurs subsequent to the TO of the reference bracket. The FEA data was validated with accuracy rates of 4.13% and 40% via using jaw displacement or strain gauge, respectively.   Based on conducted material property investigations such as mechanical tests, using Hex20 element for FEA analyses and confirmation of analyses of the bracket using a designed fixture is expected to yield more accurate results, and guide the industry and other scholars.

Author's statement
Conflict of interest: Authors state no conflict of interest. Informed consent: Informed consent has been obtained from all individuals included in this study.

References

1. E. Akca, A. Gürsel, A Review on Superalloys and IN718 Nickel-Based INCONEL Superalloy, Period. Eng. Nat. Sci. 3 (2015). https://doi.org/10.21533/pen.v3i1.43.
2. L. Scime, J. Beuth, Melt pool geometry and morphology variability for the Inconel 718 alloy in a laser powder bed fusion additive manufacturing process, Addit. Manuf. 29 (2019) 100830. https://doi.org/10.1016/j.addma.2019.100830.
3. Z. Xu, J.W. Murray, C.J. Hyde, A.T. Clare, Effect of post processing on the creep performance of laser powder bed fused Inconel 718, Addit. Manuf. 24 (2018) 486–497. https://doi.org/10.1016/j.addma.2018.10.027.
4. T. Trosch, J. Strößner, R. Völkl, U. Glatzel, Microstructure and mechanical properties of selective laser melted Inconel 718 compared to forging and casting, Mater. Lett. 164 (2016) 428–431. https://doi.org/10.1016/j.matlet.2015.10.136.
5. C. Courbon, D. Kramar, P. Krajnik, F. Pusavec, J. Rech, J. Kopac, Investigation of machining performance in high-pressure jet assisted turning of Inconel 718: An experimental study, Int. J. Mach. Tools Manuf. 49 (2009) 1114–1125.
https://doi.org/10.1016/j.ijmachtools.2009.07.010.
6. J.D. Avila, M. Isik, A. Bandyopadhyay, Titanium–Silicon on CoCr Alloy for Load-Bearing Implants Using Directed Energy Deposition-Based Additive Manufacturing, ACS Appl. Mater. Interfaces. 12 (2020) 51263–51272. https://doi.org/10.1021/acsami.0c15279.
7. M. Isik, J.D. Avila, A. Bandyopadhyay, Alumina and tricalcium phosphate added CoCr alloy for load-bearing implants, Addit. Manuf. 36 (2020) 101553. https://doi.org/10.1016/j.addma.2020.101553.
8. A. Bandyopadhyay, A. Shivaram, M. Isik, J.D. Avila, W.S. Dernell, S. Bose, Additively manufactured calcium phosphate reinforced CoCrMo alloy: Bio-tribological and biocompatibility evaluation for load-bearing implants, Addit. Manuf. 28 (2019) 312–324. https://doi.org/10.1016/j.addma.2019.04.020.
9. M.C. Chaturvedi, Y. Han, Strengthening mechanisms in Inconel 718 superalloy, Met. Sci. 17 (1983) 145–149. https://doi.org/10.1179/030634583790421032.
10. H. Williams, E. Butler-Jones, Additive manufacturing standards for space resource utilization, Addit. Manuf. 28 (2019) 676–681. https://doi.org/10.1016/j.addma.2019.06.007.
11. S. Gribbin, J. Bicknell, L. Jorgensen, I. Tsukrov, M. Knezevic, Low cycle fatigue behavior of direct metal laser sintered Inconel alloy 718, Int. J. Fatigue. 93 (2016) 156–167. https://doi.org/10.1016/j.ijfatigue.2016.08.019.
12. J.B. Bento, A. Lopez, I. Pires, L. Quintino, T.G. Santos, Non-destructive testing for wire + arc additive manufacturing of aluminium parts, Addit. Manuf. 29 (2019) 100782. https://doi.org/10.1016/j.addma.2019.100782.
13. A. Hadadzadeh, B.S. Amirkhiz, J. Li, M. Mohammadi, Columnar to equiaxed transition during direct metal laser sintering of AlSi10Mg alloy: Effect of building direction, Addit. Manuf. 23 (2018) 121–131. https://doi.org/10.1016/j.addma.2018.08.001.
14. M. Mohammadi, H. Asgari, Achieving low surface roughness AlSi10Mg_200C parts using direct metal laser sintering, Addit. Manuf. 20 (2018) 23–32. https://doi.org/10.1016/j.addma.2017.12.012.
15. E. Talay, C. Özkan, E. Gürtaş, Designing lightweight diesel engine alternator support bracket with topology optimization methodology, Struct. Multidiscip. Optim. (2021). https://doi.org/10.1007/s00158-020-02812-z.
16. M. Isik, E. Kisa, B. Koc, M. Yildiz, B. Pehlivanogullari, A. Orhangul, O. Poyraz, G. Akbulut, Topology optimization and finite elemental analysis for an inconel 718 engine mounting bracket manufactured via electron beam melting, in: 2019. https://research.sabanciuniv.edu/41130/.
17. J.-H. Zhu, W.-H. Zhang, L. Xia, Topology Optimization in Aircraft and Aerospace Structures Design, Arch. Comput. Methods Eng. 23 (2016) 595–622. https://doi.org/10.1007/s11831-015-9151-2.
18. O. Sigmund, K. Maute, Topology optimization approaches, Struct. Multidiscip. Optim. 48 (2013) 1031–1055. https://doi.org/10.1007/s00158-013-0978-6.
19. M.P. Bendsøe, O. Sigmund, Topology Optimization, Springer Berlin Heidelberg, Berlin, Heidelberg, 2004. https://doi.org/10.1007/978-3-662-05086-6.
20. M. Zhou, R. Fleury, Y.-K. Shyy, H. Thomas, J. Brennan, Progress in Topology Optimization with Manufacturing Constraints, 2002. https://doi.org/10.2514/6.2002-5614.
21. J. Liu, A.T. Gaynor, S. Chen, Z. Kang, K. Suresh, A. Takezawa, L. Li, J. Kato, J. Tang, C.C.L. Wang, L. Cheng, X. Liang, A.C. To, Current and future trends in topology optimization for additive manufacturing, Struct. Multidiscip. Optim. 57

(2018) 2457–2483. https://doi.org/10.1007/s00158-018-1994-3.

22. M. Langelaar, Topology optimization of 3D self-supporting structures for additive manufacturing, Addit. Manuf. 12 (2016) 60–70. https://doi.org/10.1016/j.addma.2016.06.010.

23. G. SHI, C. GUAN, D. QUAN, D. WU, L. TANG, T. GAO, An aerospace bracket designed by thermo-elastic topology optimization and manufactured by additive manufacturing, Chinese J. Aeronaut. 33 (2020) 1252–1259. https://doi.org/10.1016/j.cja.2019.09.006.

24. O. Giraldo-Londoño, L. Mirabella, L. Dalloro, G.H. Paulino, Multi-material thermomechanical topology optimization with applications to additive manufacturing: Design of main composite part and its support structure, Comput. Methods Appl. Mech. Eng. 363 (2020) 112812. https://doi.org/10.1016/j.cma.2019.112812.

25. T. Zhong, K. He, H. Li, L. Yang, Mechanical properties of lightweight 316L stainless steel lattice structures fabricated by selective laser melting, Mater. Des. 181 (2019) 108076. https://doi.org/10.1016/j.matdes.2019.108076.

26. P. Liu, Z. Kang, Y. Luo, Two-scale concurrent topology optimization of lattice structures with connectable microstructures, Addit. Manuf. 36 (2020) 101427. https://doi.org/10.1016/j.addma.2020.101427.

27. T. Stolarski, Y. Nakasone, S. Yoshimoto, Engineering Analysis with ANSYS Software, Elsevier Science, 2018. https://books.google.com.tr/books?id=50IyDwAAQBAJ.

28. J. Jung, S. Goo, J. Kook, Design of a local resonator usin topology optimization to tailor bandgaps in plate structures, Mater. Des. 191 (2020) 108627. https://doi.org/10.1016/j.matdes.2020.108627.

29. M. Seabra, J. Azevedo, A. Araújo, L. Reis, E. Pinto, N. Alves, R. Santos, J. Pedro Mortágua, Selective laser melting (SLM) and topology optimization for lighter aerospace componentes, Procedia Struct. Integr. 1 (2016) 289–296. https://doi.org/10.1016/j.prostr.2016.02.039.

30. J. París, F. Navarrina, I. Colominas, M. Casteleiro, Topology optimization of continuum structures with local and global stress constraints, Struct. Multidiscip. Optim. 39 (2009) 419–437. https://doi.org/10.1007/s00158-008-0336-2.

31. M. Langelaar, An additive manufacturing filter for topology optimization of print-ready designs, Struct. Multidiscip. Optim. 55 (2017) 871–883. https://doi.org/10.1007/s00158-016-1522-2.

32. A. Ramos, J.A. Simões, Tetrahedral versus hexahedral finite elements in numerical modelling of the proximal femur, Med. Eng. Phys. 28 (2006) 916–924. https://doi.org/10.1016/j.medengphy.2005.12.006.

33. D. Burkhart, B. Hamann, G. Umlauf, Iso-geometric Finite Element Analysis Based on Catmull-Clark : ubdivision Solids, Comput. Graph. Forum. 29 (2010) 1575–1584. https://doi.org/10.1111/j.1467-8659.2010.01766.x.

34. B. Roith, A. Troll, F. Rieg, Integrated finite element analysis (FEA) in three-dimensional computer aided design programs (CAD) - Overview and comparison, in: Proc. ICED 2007, 16th Int. Conf. Eng. Des., INTERNATIONAL CONFERENCE ON ENGINEERING DESIGN, ICED'07, Paris, 2007.

35. J. Wulff, Structure and Properties of Materials: Mechanical behavior, by H.W. Hayden, L.G. Moffatt, and J. Wulff, Wiley, 1964. https://books.google.com.tr/books?id=pdLPBH9YbW4C.

36. T.H. Courtney, Mechanical Behavior of Materials, McGraw-Hill, 2000. https://books.google.com.tr/books?id=hqDgAAAAMAAJ.